Flow structures and sandbar dynamics in a canyon river during a controlled flood, Colorado River, Arizona

Scott A. Wright[1] and Matt Kaplinski[2]

Received 6 July 2009; revised 23 September 2010; accepted 20 September 2010; published 8 March 2011.

[1] In canyon rivers, debris fan constrictions create rapids and downstream pools characterized by secondary flow structures that are closely linked to channel morphology. In this paper we describe detailed measurements of the three-dimensional flow structure and sandbar dynamics of two pools along the Colorado River in the Grand Canyon during a controlled flood release from Glen Canyon Dam. Results indicate that the pools are characterized by large lateral recirculation zones (eddies) resulting from flow separation downstream from the channel constrictions, as well as helical flow structures in the main channel and eddy. The lateral recirculation zones are low-velocity areas conducive to fine sediment deposition, particularly in the vicinity of the separation and reattachment points and are thus the dominant flow structures controlling sandbar dynamics. The helical flow structures also affect morphology but appear secondary in importance to the lateral eddies. During the controlled flood, sandbars in the separation and reattachment zones at both sites tended to build gradually during the rising limb and peak flow. Deposition in shallow water on the sandbars was accompanied by erosion in deeper water along the sandbar slope at the interface with the main channel. Erosion occurred via rapid mass failures as well as by gradual boundary shear stress driven processes. The flow structures and morphologic links at our study sites are similar to those identified in other river environments, in particular sharply curved meanders and channel confluences where the coexistence of lateral recirculation and helical flows has been documented.

Citation: Wright, S. A., and M. Kaplinski (2011), Flow structures and sandbar dynamics in a canyon river during a controlled flood, Colorado River, Arizona, *J. Geophys. Res.*, *116*, F01019, doi:10.1029/2009JF001442.

1. Introduction

[2] The interaction between flow structures and channel boundaries is of primary importance in studies of river form and process. Because of this importance, substantial research has been directed at measuring and modeling these flow structures and associated channel morphodynamics in a range of channel environments, including straight channels, braided rivers, meander bends, channel confluences, pool-riffle units, and groyne fields, among others. However, there is a relative lack of information for canyon rivers, particularly with respect to three-dimensional flow structures. Herein we begin to fill this gap by presenting detailed measurements of flow structures and sandbar morphodynamics along the Colorado River in the Grand Canyon (Figure 1) during a controlled flood release from Glen Canyon Dam.

[3] The two most common secondary flow structures in rivers are helical flows and lateral recirculation zones (also commonly referred to as eddies and gyres). Helical flows result from the interaction between vertical gradients in momentum and topography, and appear as circulations in the lateral-vertical plane (i.e., oriented perpendicular to downstream flow). These structures have been observed in many environments (including straight channels), but those with most relevance for our study are found in meander bends and channel confluences. The curvature-induced helix and its effects on the morphology of meandering rivers (i.e., outer bend erosion and point bar deposition) have been the subject of extensive research [e.g., *Bathurst et al.*, 1977; *Dietrich et al.*, 1979; *Dietrich and Smith*, 1983, 1984; *Thorne and Rais*, 1985]. Similar helical flow structures have been observed at channel confluences [*Ashmore et al.*, 1992; *Rhoads and Kenworthy*, 1995]. Though curvature can play a role at confluences, *Bradbrook et al.* [1998] showed that it is not required and that the development of helical flow depends primarily on momentum and depth differences between the adjoining streams. Helical flows have also been linked to near-bed velocities that route sediment away from the deepest pools in the pool-riffle unit [*Booker et al.*, 2001], thus contributing to the maintenance of this geomorphic form. Lateral recirculation zones have been observed in many of these same settings, but originating from a different process: flow separation. In sharply curving

[1]U.S. Geological Survey, Sacramento, California, USA.
[2]Department of Geology, Northern Arizona University, Flagstaff, Arizona, USA.

0148-0227/11/2009JF001442

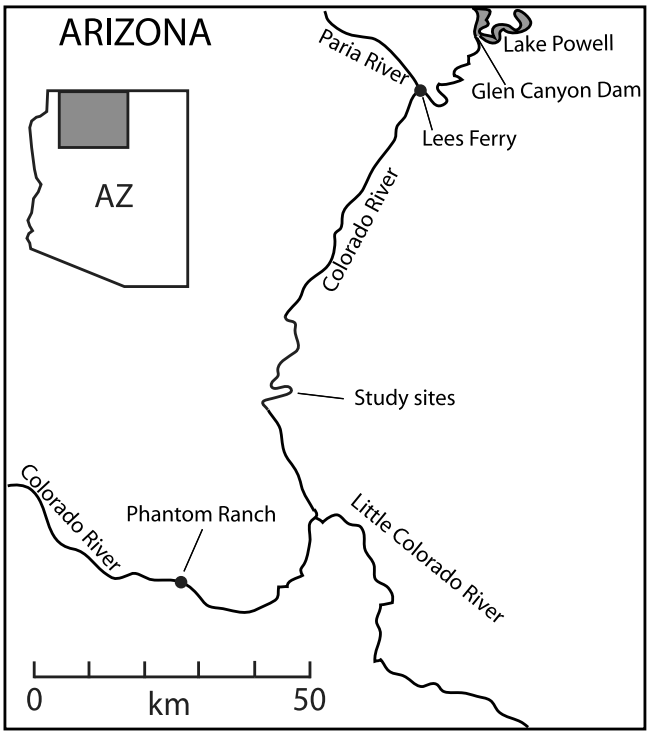

Figure 1. Map of the Colorado River below Glen Canyon Dam showing the location of the study sites.

meander bends, flow separation may occur along the inner bank at the bend apex resulting in a zone of low-velocity, lateral recirculating flow [*Leeder and Bridges*, 1975; *Hodskinson and Ferguson*, 1998; *Ferguson et al.*, 2003]. Flow separation and lateral recirculation have also been observed at an asymmetrical channel confluence [*Rhoads and Kenworthy*, 1995]. *Thompson et al.* [1996] and *Booker et al.* [2001] showed that channel constrictions at pool heads can lead to downstream flow separation and laterally recirculating flow within pool-riffle units. Finally, lateral recirculation zones are a common feature of some river engineering works; studies of groyne fields [e.g., *Sukhodolov et al.*, 2002] have particular relevance to our study.

[4] Though little is known about the details of the three-dimensional flow structure in canyon rivers, many studies have examined the basic hydraulics and links to morphology. In bedrock-confined rivers, the fundamental geomorphic structure (rapids and pools) is set by the tributary debris fans that create the rapids. However, substantial erosion and deposition of fine sediment occurs in areas that are closely linked to secondary flow structures. For example, *Howard and Dolan* [1981], *Schmidt* [1990], *Schmidt and Graf* [1990], and *Rubin et al.* [1990] described the basic flow structures and morphologic linkages for the Colorado River in Grand Canyon (Figure 1; this reach contains our study sites). *Schmidt* [1990] described the basic geomorphic unit as the "fan-eddy complex" because tributary debris fans constrict the main channel and the expansions result in flow separation and zones of lateral recirculation, or eddies (Figure 2). At some distance downstream the flow decelerates and reattaches to the bank leading to fine sediment deposition and the development of a "reattachment bar" that projects in an upstream direction into the eddy [*Rubin et al.*, 1990]. It is also common for a secondary eddy to form immediately downstream from the separation point, also resulting in fine sediment deposition and development of a "separation bar" (Figure 2). These flow structures and deposition patterns have been documented extensively for the Colorado River in Grand Canyon as well as for other rivers where tributary debris fans constrict the main channel [*Schmidt et al.*, 1995; *Grams and Schmidt*, 1999; *Schmidt and Rubin*, 1995; *Andrews and Vincent*, 2007; *Vincent and Andrews*, 2008]. Two-dimensional (depth-averaged) numerical models have reproduced flow separation, lateral recirculation, and depositional patterns in these environ-

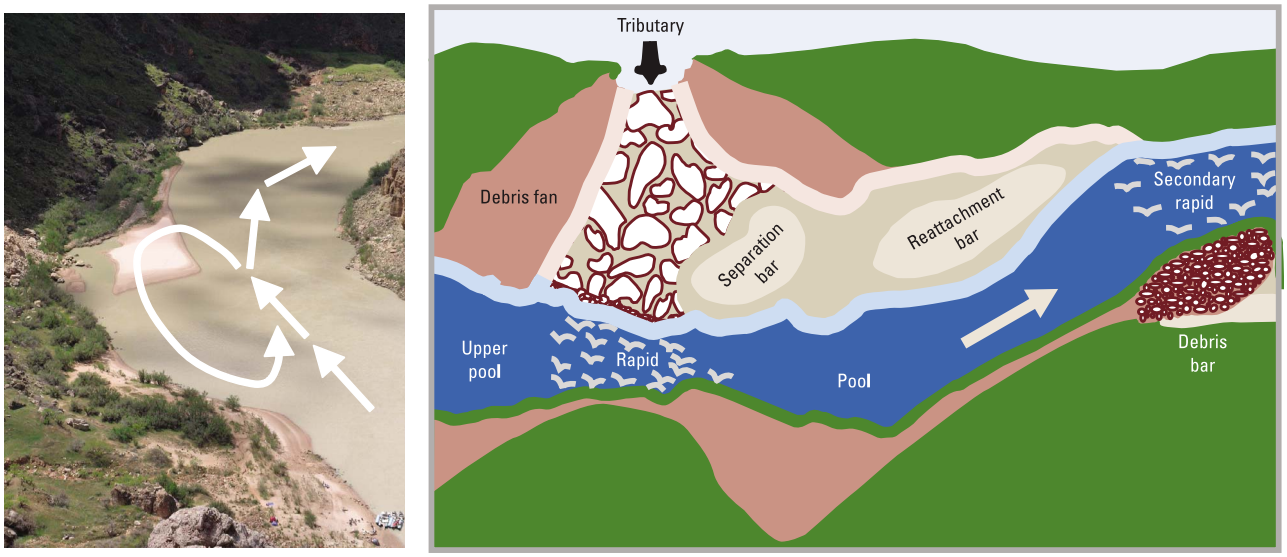

Figure 2. (left) Photograph of the EM study site and (right) schematic of a fan-eddy complex along the Colorado River below Glen Canyon Dam. Figure 2 (right) reproduced from *Webb et al.* [2005].

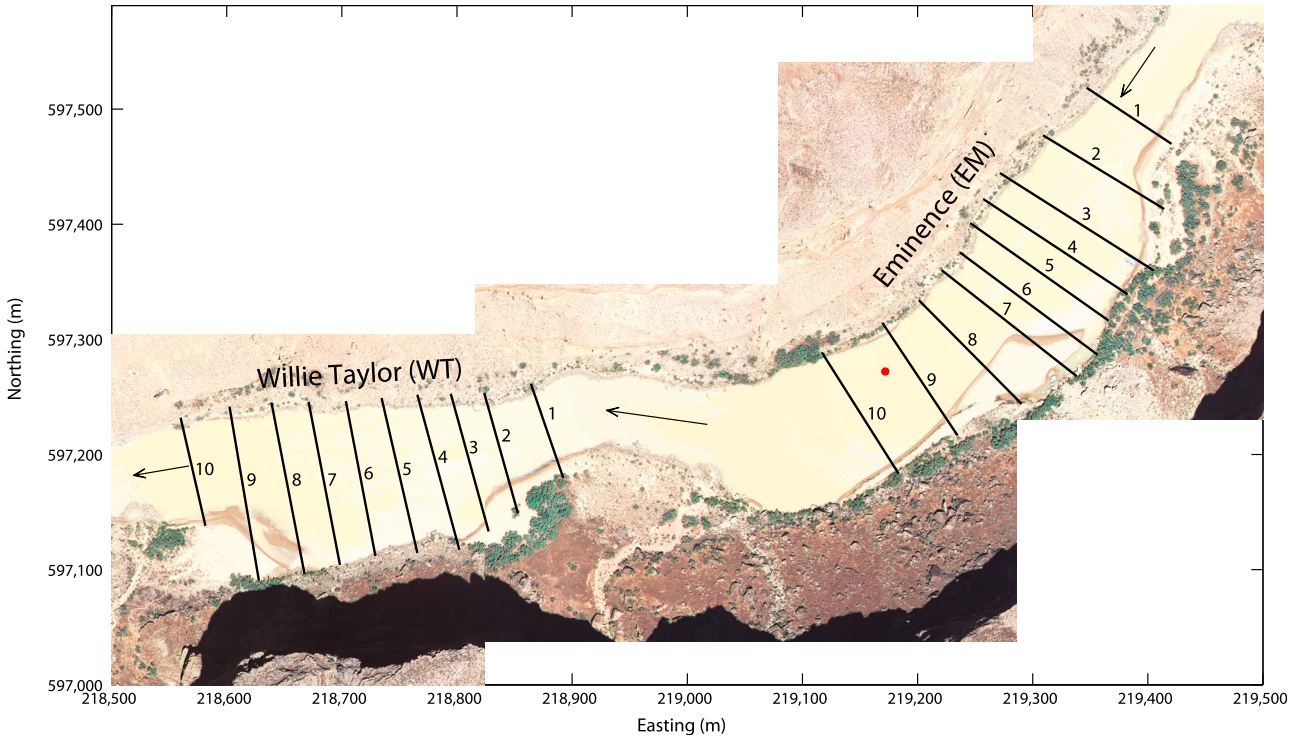

Figure 3. Aerial photography of the study sites showing transect lines for the ADCP surveys and the location (red dot) of the suspended-sediment sampling. Flow is from top right to bottom left. Photography is from May 2005 at a water discharge of ~227 m^3/s.

ments [*Wiele et al.*, 1996, 1999; *Miller*, 1994]; however, these models have not been compared to measured flow fields because data have previously been unavailable.

[5] Herein we describe a set of detailed measurements of the three-dimensional flow structure and sandbar dynamics in two pools below rapids along the Colorado River in Grand Canyon National Park, Arizona, USA, during a controlled flood release from Glen Canyon Dam in March 2008. Our objectives here are to describe (1) the flow structures observed at the two sites, their dependence on flow rate, and their similarities with flow structures in other river environments; (2) the sandbar dynamics of the two sites, including the rates and styles of erosion and deposition throughout the flood; and (3) describe the linkages between the observed flow structures and sandbar dynamics, within the context of similar linkages in other riverine settings.

2. Study Site and Methods

[6] Repeated measurements of river bathymetry, velocity profiles, and suspended-sediment concentrations were made at two fan-eddy complexes during the controlled flood release from Glen Canyon Dam in March 2008. The study sites are located approximately 97 km downstream from the dam (Figure 1). Each fan-eddy complex consists of a tributary debris fan that constricts the main channel leading to flow separation downstream, recirculation, and sandbar development in the separation and reattachment zones. The upstream study site (Figure 3) is commonly referred to as "Eminence Break" and the downstream study site as "Willie Taylor"; for the sake of brevity, herein we refer to the sites as EM and WT, respectively (Figure 3). The flood hydrograph consisted of a rise from 300 to 1200 m^3/s in about 1.5 days, followed by a steady peak of 1200 m^3/s for 2.5 days. The hydrograph at our study sites (shown in Figures 10 and 12) was estimated by routing flows from the nearest flow gage (~24 km upstream) using the model of *Wiele and Griffin* [1997]. The peak release has a recurrence interval of slightly less than 1 year based on predam flow data (pre-1965) [*Topping et al.*, 2003]; postdam, flows above power plant capacity (900 m^3/s) have only occurred a few times and for multiple purposes. Thus, while not large compared to most predam annual floods, the controlled flood peak is infrequent and geomorphically significant.

[7] Bathymetry was surveyed with a multibeam sonar system (Reson Seabat 8124 sonar with TSS MAHRSS reference system for heave, pitch, roll, and heading) deployed from a motorized inflatable raft. Because global positioning systems are unreliable in Grand Canyon, boat position and elevation were tracked using a robotic total station. Areas above water and shallow areas near the shoreline were surveyed with conventional total station techniques. The multibeam and conventional surveys were combined and converted to 1 m grids to facilitate volumetric change calculations by differencing the gridded surfaces. The conventional survey point density was about 0.5 to 1 points/m^2 and the multibeam density varied from 10 to 1000 points/m^2 depending on boat speed and sweep overlap. Error bars for volume change calculations were computed based on a thresholding technique [e.g., *Wheaton et al.*, 2009] for evaluating differences that are less than the uncertainty in

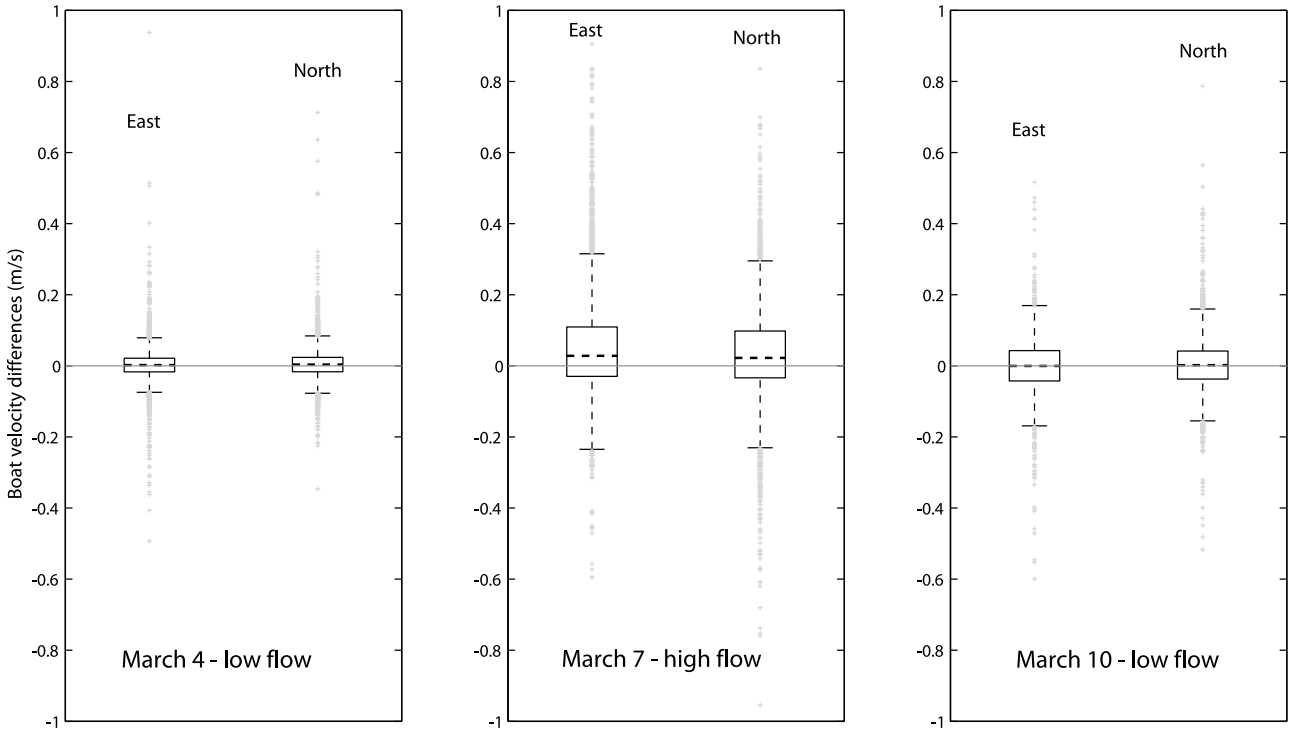

Figure 4. Differences between boat velocities from bottom tracking and boat velocities derived from total station positions for three surveys at EM. Differences are slightly higher and biased positive at high flow due to bed movement.

the measurement. A priori estimates of DEM uncertainty were developed using the methods described by *Calder and Mayer* [2003]. We also directly compared DEMs over areas assumed not to have changed, such as gravel bars and bedrock. The a priori technique yielded a 95% root mean square (RMS) uncertainty estimate of 23 cm and the direct DEM differences ranged from 8 to 10 cm at 95% RMS. Thus, we set the uncertainty threshold conservatively at 25 cm, and for each surface difference the error bar was estimated as the sum (signed) of all differences below the threshold. Though accounting for measurement uncertainty is clearly important in general for DEM differencing, for our study the magnitudes of the changes were substantially larger than the measurement uncertainty. The surveying techniques are described in detail by *Hazel et al.* [2008] and *Kaplinski et al.* [2009]. Surveys were typically performed twice per day at each site, yielding 15 surveys of EM and 12 surveys of WT. Results for DEM differences are reported as volumetric changes between the two surfaces; these volume changes can be converted to average elevation changes using the total areas of the surveys (EM area = 53,100 m^2, WT area = 36,500 m^2).

[8] Vertical profiles of suspended-sediment concentration were collected in the main channel at the lower end of EM (Figure 3) approximately once per day (8 total profiles). Each profile consisted of triplicate samples at four positions within the flow depth (finer spacing nearer the bed). All samples were collected with a USGS P-61 point integrating sampler [*Edwards and Glysson*, 1999]. The samples were processed for concentration using standard gravimetric methods [*Guy*, 1969] and for grain size distribution (sand only, 1/4-phi increments) using a sieve-calibrated Beckman Coulter LS 100Q laser-diffraction particle size analyzer. Depth-averaged sand concentrations were computed by fitting Rouse-form profiles [e.g., *Vanoni*, 1975] to the measured data and integrating from the water surface to near the bed (within 5% of flow depth).

[9] Velocity profiles were collected with an acoustic Doppler current profiler (ADCP, RD Instruments Workhorse Rio Grande, 600 kHz) deployed from a motorized, inflatable raft. Profile data were collected along ten transects at each site (Figure 3) approximately twice daily, yielding 12 surveys of EM and 11 surveys of WT. Transects were laid out on imagery prior to the survey with the goal of transects perpendicular to the primary downstream (streamwise) flow. During the surveys, onboard data acquisition software (Hypack) was used to display the boat position and transect line in real time, allowing the boat operator to maintain boat position along each transect typically to within a few meters. As with the bathymetry surveys, boat position was tracked using a robotic total station. Postprocessing of the data included computing boat velocities from the total station position information and using these velocities to correct the raw velocity data from the ADCP instrument. This was necessary because moving-bed conditions in the river biased bottom tracking boat velocities, particularly during the peak flow, and also provided absolute positions in earth coordinates (bottom tracking only provides relative positions). We checked our total station boat velocity calculations through comparisons with bottom tracking velocities

and found excellent agreement. Figure 4 shows box plots of the differences between bottom tracking velocities and total station derived velocities for three surveys at EM. It is seen that the differences between the two methods are very small, particularly for the low flows when bed movement was minimal (bed movement is apparent in the high-flow survey yielding slight positive bias). For the three surveys, the differences in velocities had median values of 0.0028, 0.025, and 0.00085 m/s, respectively, with standard deviations of 0.046, 0.15, and 0.078 m/s. These small differences between the two methods confirm that the ADCP compass was properly calibrated and functioning correctly. The differences in boat velocities between the methods are orders of magnitude smaller than typical measured water velocities.

[10] For all surveys, data were collected using a vertical bin size of 33 cm and a ping rate of approximately 2 Hz. Two traverses were conducted at each transect with boat speeds typically on the order of 1 m/s in order to facilitate temporal and spatial averaging. While more traverses at each transect would obviously be more desirable for obtaining the mean flow properties [*Szupiany et al.*, 2007], our approach represents a compromise between the need for temporal averaging and the desire to map the spatial structure in detail in a rapidly changing environment. Our spatial and temporal averaging consisted of mapping the individual-ping ADCP data onto 10 m lateral grids along each transect. That is, we broke each transect into 10 m segments and averaged all pings collected within that segment (thus each average includes data from traverses in opposite directions across the channel). Because our boat speed averaged around 1 m/s and we made two passes, this resulted in about 20 s of data (40 pings) for each 10 m segment. We evaluated the error resulting from this temporal averaging using stationary data collected during suspended sediment sampling. Herein we report the results from data collected on 7 March during the peak flow for a middepth location in the profile; analyses from other sampling days and locations within the profile yielded similar results. Data were collected at the suspended sediment sampling location (Figure 3) for approximately 30 min. The averages over this 30 min period for the three velocity components were 1.1, 0.47, and 0.008 m/s respectively, for east, north, and vertical directions. To evaluate our averaging errors, we computed moving averages over the time series using a 40 ping window (i.e., the typical number of pings in our averages), and differenced these with the "true" averages over the entire time series. This yielded median absolute errors of 0.11, 0.082, and 0.022 m/s for east, north, and vertical directions, respectively. The potential impact of these errors on interpretation of flow structures was evaluated by comparing them with averaged velocity data from the full survey on 7 March. The fundamental question is whether these errors could be large enough to yield flow patterns opposite to their true directions. Thus we computed the number of averaged measurements that fell below the error thresholds for both horizontal and vertical components. The 7 March survey yielded 4,972 averaged horizontal velocity measurements with 4,762 of these (~96%) exceeding the approximate horizontal velocity error of 0.1 m/s. Thus, we believe it highly unlikely that these averaging errors could lead to misinterpretation of horizontal flow structures. For vertical velocities, the survey yielded 2,486 measurement with 1,992 of these (~80%) exceeding our estimated median vertical velocity error of 0.022 m/s. Though not as conclusive as the analysis of horizontal errors, these results indicate that only a relatively small percentage of vertical velocity measurement may be in the wrong direction and thus are unlikely to confound interpretations of large-scale flow structures.

3. Results: Flow Structures

3.1. Lateral Recirculation

[11] As expected, both sites exhibited lateral recirculation zones downstream from the debris fan constrictions, and these structures persisted at both low and high flow (Figure 5). The style of lateral recirculation changed substantially with flow rate, but in different ways at the two sites. Flow velocities increased substantially from low to high flow; for the fourfold increase in discharge during the flood, velocities (depth-averaged) increased by about a factor of 2.5 (on average). Accompanying these changes in velocity were changes in the shapes of the recirculation zones, with a general trend of the eddies becoming thinner and longer at high flow. For example, at EM the eddy eye (i.e., the center of the main circulation) and the reattachment point both moved downstream and away from the main channel (Figure 5, locations were estimated by visual inspection). WT exhibited a similar response with the eddy eye and reattachment point moving away from the main channel; however, the reattachment point moved only very slightly downstream because the eddy is pinned against another debris fan (Figures 3 and 5). Another difference between low and high flow was the development of a smaller "separation" eddy upstream from the primary eddy. This is clearly evident at WT (Figure 5) but more difficult to distinguish at EM. Direct visual observation in the field suggested that there was some weak circulation in the separation zone at EM that wasn't resolved by our grid. This organization, that is, two eddies side-by-side rotating in opposite directions was described by *Schmidt* [1990] for Grand Canyon and is quite similar to that found in flume experiments of groyne fields [*Uijttewaal et al.*, 2001; *Sukhodolov et al.*, 2002]. The geometries of our sites (e.g., debris fan spacing and constriction ratio) are such that they fall well below the defined threshold in groyne fields for transition to a single circulation cell [*Sukhodolov et al.*, 2002].

3.2. Three-Dimensional Flows

[12] The three-dimensional structure of the flow is best visualized through cross-sectional panels (at the ADCP transects) showing all three velocity components (Figures 6 and 7). In Figures 6 and 7, the downstream and cross-stream velocity components are defined as being perpendicular and parallel, respectively, to each ADCP transect (refer to Figure 3 for cross-section numbers). As noted in section 2, the ADCP transects were drawn on imagery prior to the survey. The goal was to draw transects perpendicular to the main downstream flow; however, without prior knowledge of the details of the flow structure this is nearly impossible. Thus, some skewness in the cross-section data is readily apparent in Figures 6 and 7, whereby the cross-stream velocities may be oriented in the same direction across the

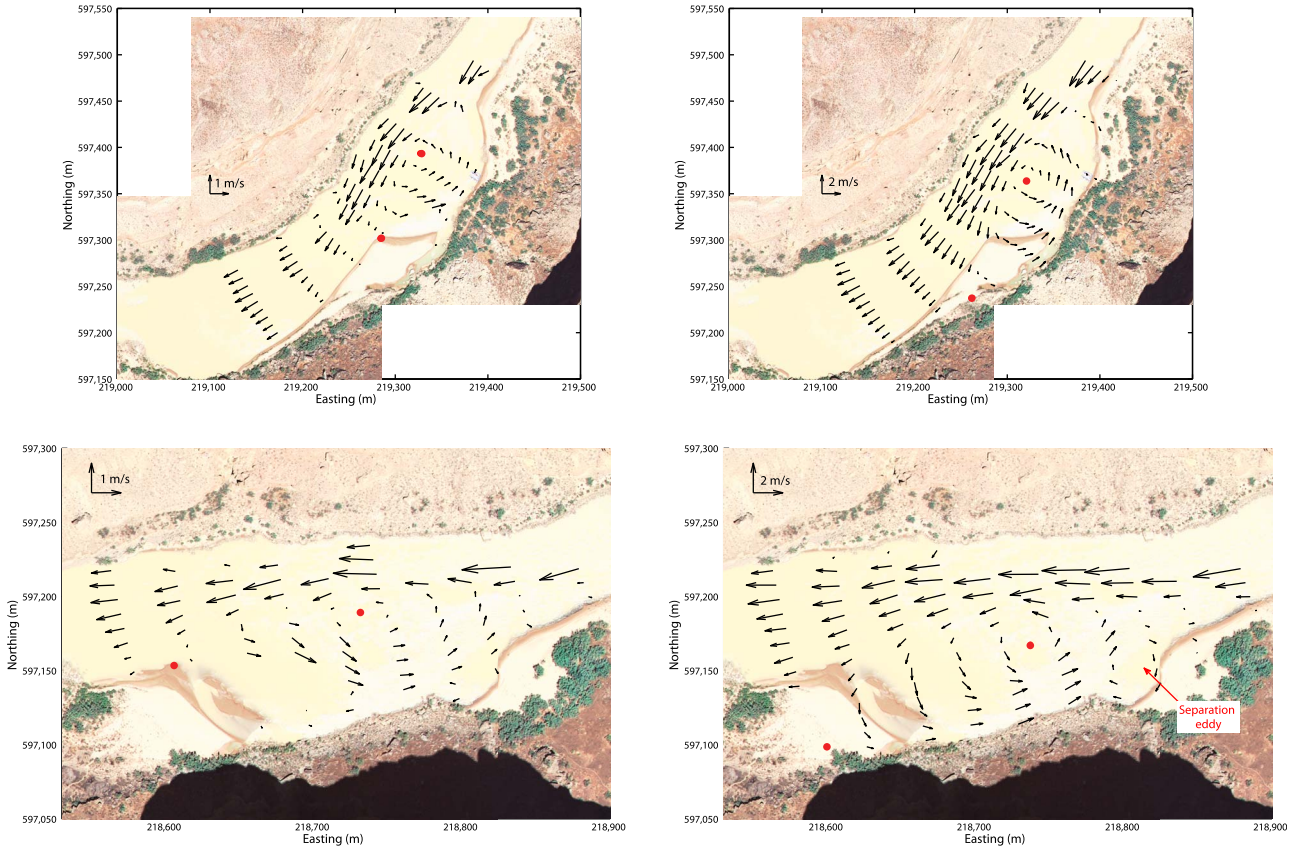

Figure 5. Depth-averaged horizontal velocities for both sites ((top) EM and (bottom) WT) at (left) low flow (after flood recession on 10 March) and (right) during the peak flood flow (7 March). Note the difference in velocity scale (factor of 2) between the low flow and peak flow. Red dots represent approximate locations of the eddy eye and reattachment point.

entire channel (i.e., the cross-stream flux does not sum to zero across the section). Ideally the cross sections could be rotated to minimize this skewness, but since the velocity data are only available along the transects this is not possible. While we do not believe that the secondary flow structures described below are a direct result of this skewness, it should be kept in mind when interpreting Figures 6 and 7.

[13] Several features of interest are apparent from these cross-section views. First, the lateral recirculation zones are seen to affect and interact with the main downstream flow. In the areas where the eddy flows reconverge with the main channel (e.g., panels EM3, EM4, WT4, WT5), substantial cross-stream velocities develop that force the high-velocity core of the downstream flow toward the right bank. This can best be seen at the EM site (Figure 6); very high downstream velocities precluded boat access along the right bank at WT. This cross-stream forcing is apparent at low and high flow; however it is much stronger at high flow. Depth differences between eddy return flows (which are shallower) and the main channel lead to a high-velocity core that is tilted to the right from the bed to the surface (e.g., panel EM5); that is, the eddy return flows preferentially affect the near surface main channel flows. This confluence between the main channel and eddy return flow also produces helical flow structures in the main channel at high flow. These can be seen in panels EM3–EM4 and WT4–WT5 (between stations 40–60 m in each panel). The physical setting suggests that these helical flows are the result of a combination of mechanisms acting in meander bends and at channel confluences. The eddy return flow must curve toward downstream due to the right bank (and aided by the downstream flow), but the return flow also creates substantial cross-stream flow in the main channel that can lead to helical motions [*Bradbrook et al.*, 2000]. These structures are not apparent at low flow (or are much weaker and more difficult to measure), which suggests that the cross-stream momentum transfer is too weak to induce helical flow.

[14] Further downstream past the eye of the main eddy, cross-stream flow switches direction and is oriented into the eddy. At EM, this transition moves downstream as flow increases whereas at WT the transition is nearly stationary longitudinally (as noted in the previous section). The cross-stream and vertical flows tend to accelerate up and over the reattachment sandbars, then decelerate as the left banks and the return current channels (see Figure 2) are approached. The cross-stream velocities cause the formation of helical flow structures in the return current channels that are similar in nature to those in the main channel. These structures are best illustrated in the WT7 and WT8 panels (between stations 100–140 m), but are also visible in panels EM5 and

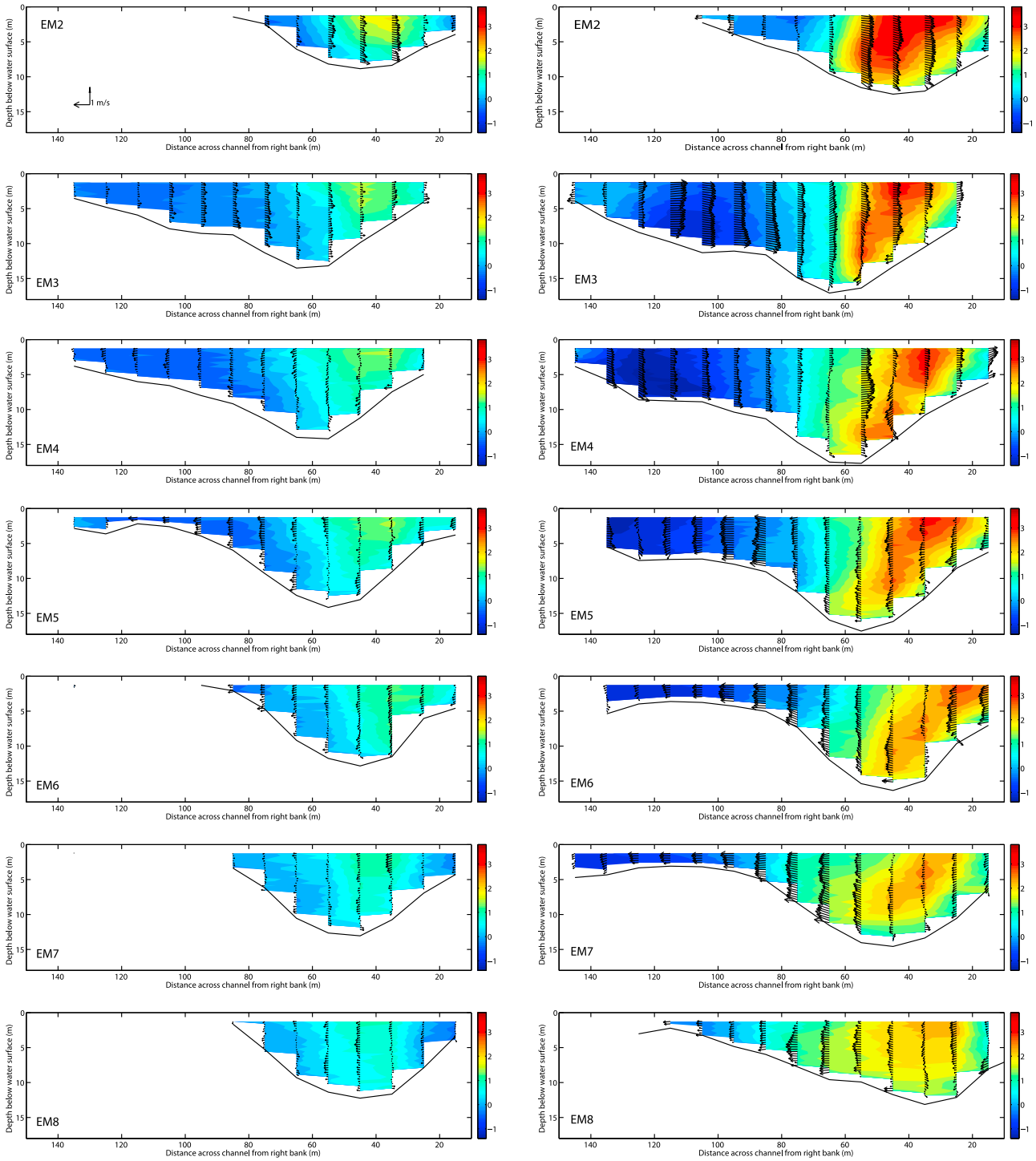

Figure 6. Cross-section views of EM ADCP transects at (left) low and (right) peak flow. The view is looking downstream. Filled contours are the downstream velocity component (downstream flow is red, upstream is blue). Arrows show vectors of cross-stream and vertical velocity components. Cross-section numbers are shown in Figure 3 for reference. For comparison, all scales are identical in each panel.

EM6. Like the main channel structures, it is likely that the underlying mechanisms are a combination of curvature-and confluence-induced cross-stream momentum transfer. The return current channels curve away from the reattachment points to carry flow upstream along the left bank (blue filled contours), but they also receive lateral flows coming across the sandbars along their lengths. Cross sections EM7 and WT8 show that the sandbar surfaces are elevated above the beds of the return current channels potentially setting up the

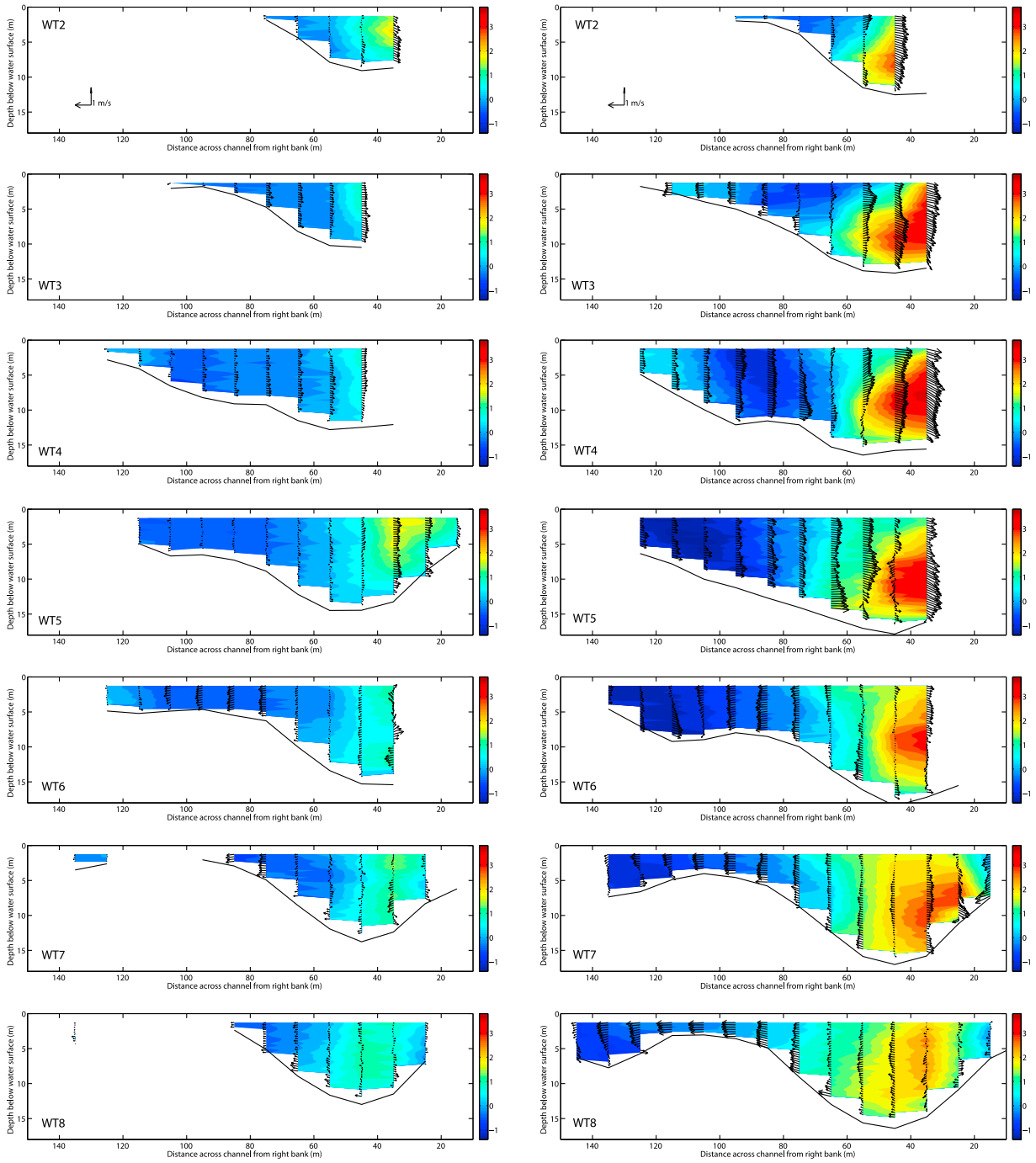

Figure 7. Cross-section views of transects at WT at (left) low and (right) peak flow. Details are described in Figure 6 caption.

depth differences necessary to induce helical motion at confluences [*Bradbrook et al.*, 2000].

4. Results: Sandbar Dynamics

4.1. Overview of Morphologic Changes During the Flood

[15] The patterns and magnitudes of morphologic change are shown in Figure 8, which contains preflood and postflood bathymetric maps and their differences, for both sites. The difference maps reveal several similarities and differences between the morphologic responses at the two sites. Both sites experienced deposition around the reattachment point and extending upstream into the eddy, that is, building of the reattachment bars. Both sites also experienced deposition in the zones of separation immediately below the constrictions, that is, building of the separation bars (see Figure 2 for definitions). Both sites were subject to erosion along the lateral sandbar slopes at the interface between the main channel and the eddies, as well as within the return

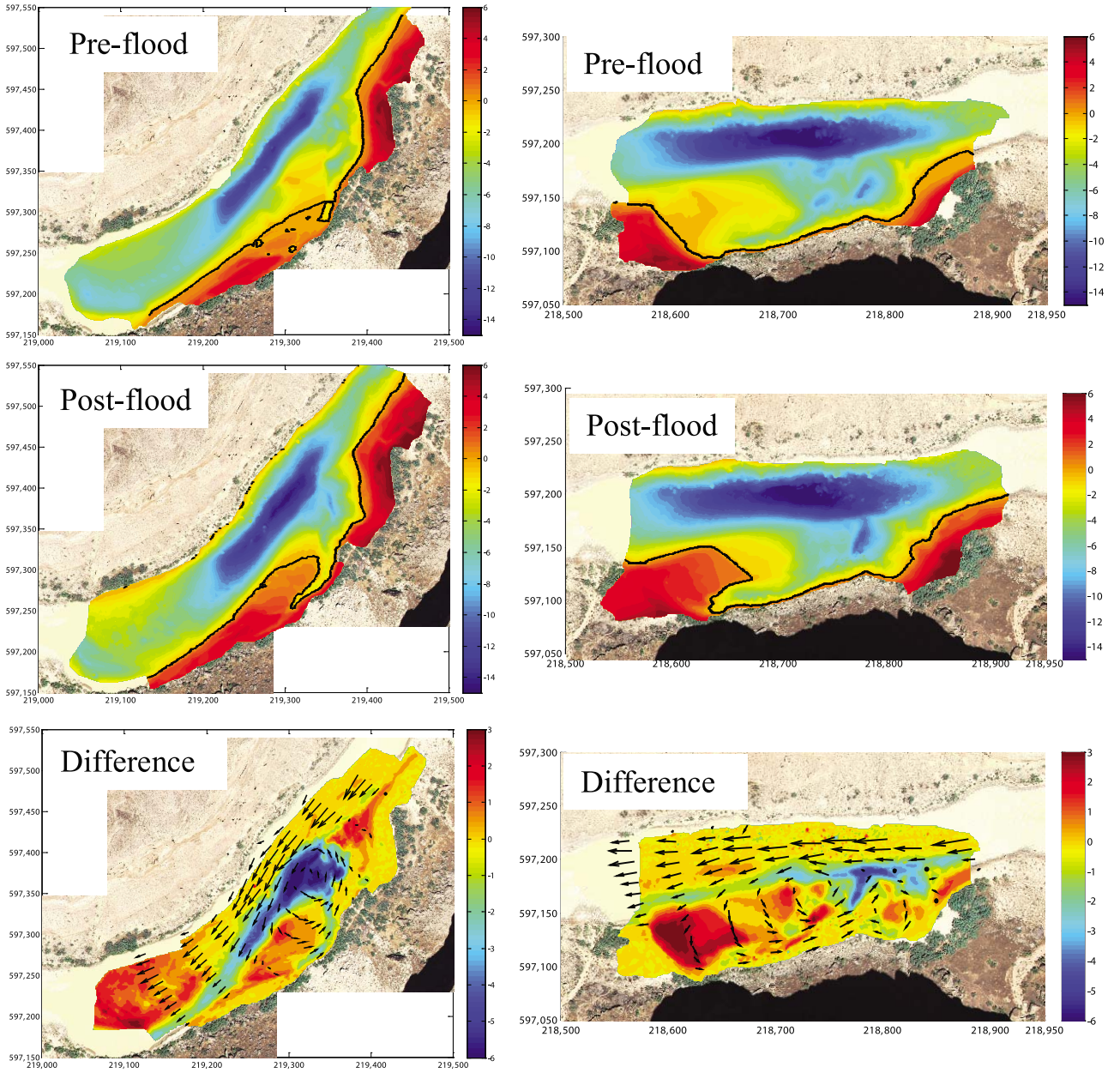

Figure 8. (top) Preflood and (middle) postflood bathymetry for both sites (elevations in meters relative to the 227 m^3/s water surface elevation) and (bottom) difference maps showing areas of erosion (blue) and deposition (red) in meters. Velocity vectors are depth averages at high flow. Black contour lines in the bathymetric maps are the 227 m^3/s water surface elevations.

current channels. The primary difference in the response was the large scour hole that developed in the proximity of the eddy eye (at high flow) at EM. The WT site also experienced substantial erosion in the area where the return current channel reconnects with the main stem, but this erosion was less in magnitude and further upstream than at EM (deposition occurred around the high-flow eddy eye at WT). These differences in erosion magnitude result in the EM site being net erosional during the flood (−11,073 ± 503 m^3) while the WT site was net depositional (2,304 ± 303 m^3).

[16] In Figure 8, elevations are referenced to the water surface elevation at 227 m^3/s [from *Hazel et al.*, 2006a] because this flow is typically the lowest release from Glen Canyon Dam and it thus provides a convenient approximate dividing line between sand above and below "baseflow." One of the goals of the controlled floods is to transfer sand from low elevation (i.e., below base flow), where it may accumulate during typical dam operations, to subaerially exposed sandbars [*Schmidt*, 1999; *Andrews et al.*, 1999]. To evaluate this transfer for our sites, we computed volume changes between surveys within individual 25 cm vertical layers as follows:

$$dV_i = (V_{bi} - V_{ti})|_{s2} - (V_{bi} - V_{ti})|_{s1} \quad (1)$$

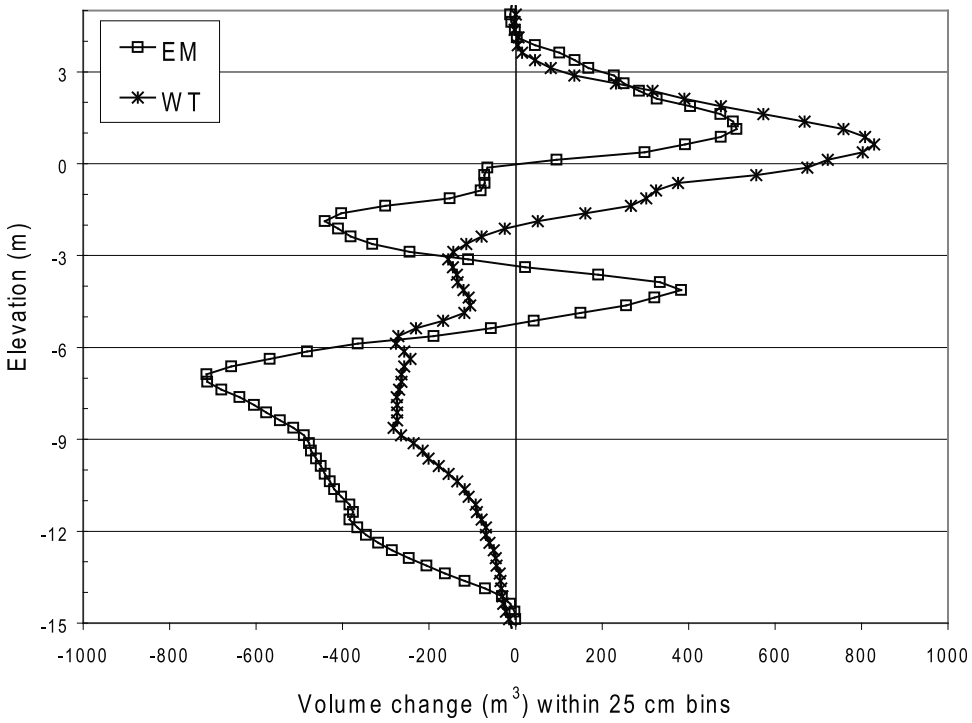

Figure 9. Volume changes over the flood as a function of elevation for both sites illustrating the trend of erosion at low elevation accompanied by deposition at high elevation.

where dV_i is the change in volume within layer i, between two surveys (s2 and s1), and V_{bi} and V_{ti} denote the total volume above the bottom and top of layer i, respectively. This allows for evaluation of volume changes as a function of elevation, as shown in Figure 9. The results indicate that this transfer did occur, with deposition prevailing at the higher elevations and erosion prevailing at lower elevations. It is also seen that the transition from erosion to deposition tended to occur near the 227 m^3/s elevation (zero in Figure 9), suggesting that this is indeed a reasonable dividing line for evaluating the transfer. The results also reinforce the findings from Figure 8 that EM experienced substantially more erosion from low elevation, while deposition was greater at high elevation at WT.

[17] The time evolution of volume change for each site is shown in Figure 10 (along with the flood hydrograph), where the trend for deposition at high elevation and erosion at low elevation is again apparent. As noted, both sites experienced erosion at low elevation and Figure 10 (left) shows that this erosion proceeded at a nearly constant rate at EM, while at WT almost all of the erosion occurred on the rising limb of the flood, resulting in substantially more erosion at EM. At high elevation, deposition rates were relatively constant at both sites through the rising limb and peak flow (Figure 10, right), with erosion occurring during the flood recession. It is again apparent from Figure 10 (right) that deposition at WT was significantly greater than at EM.

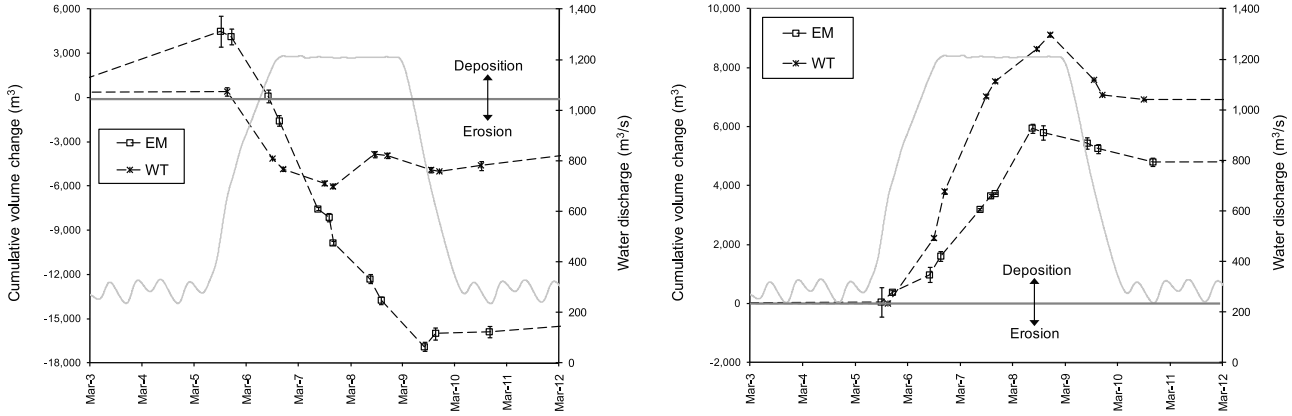

Figure 10. Cumulative volume changes through time for both sites for (left) low elevation (below 227 m^3/s) and (right) high elevation. Flood hydrograph is shown in the background.

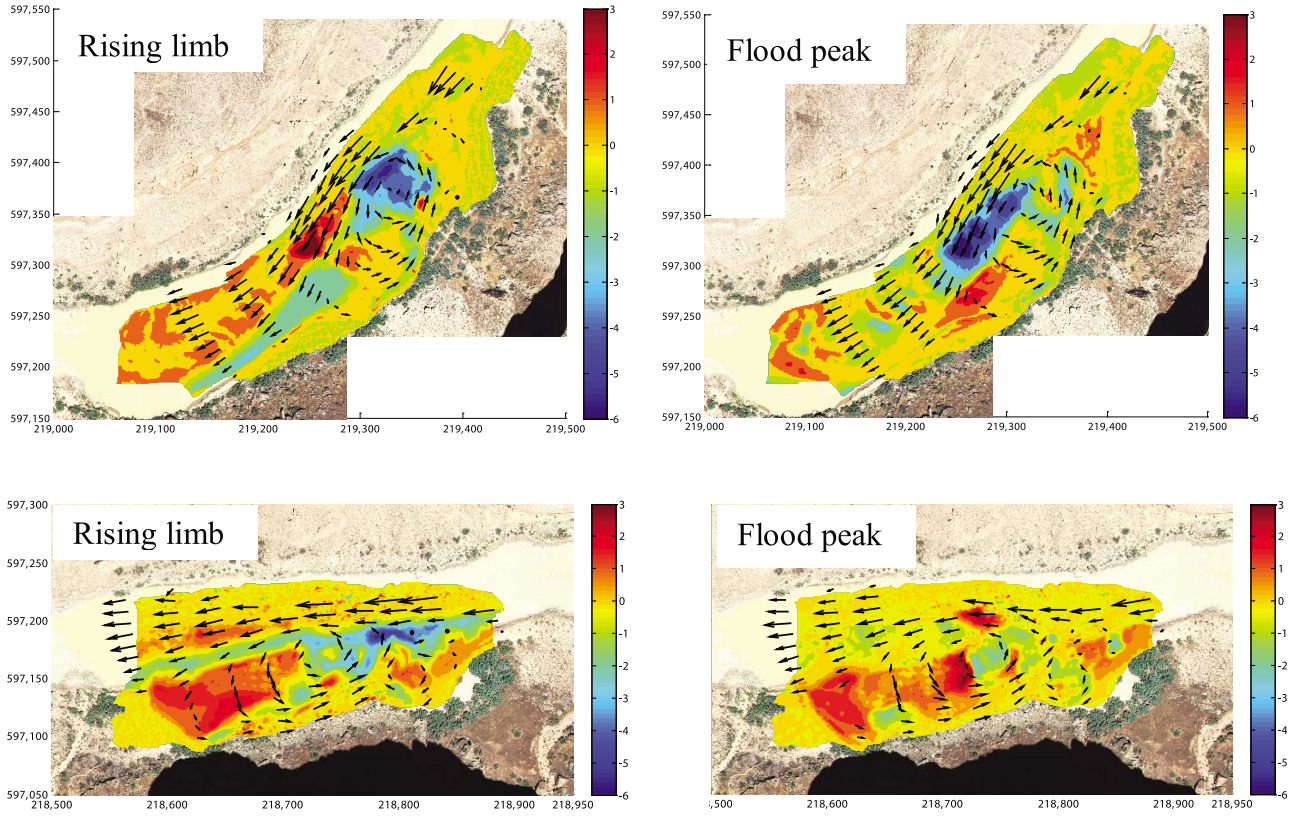

Figure 11. Difference maps (meters) for (top and bottom) the two sites for two components of the flood hydrograph: (left) the rising limb (~1.5 day duration) and (right) the peak (~2.5 day duration).

4.2. Styles of Erosion and Deposition

[18] Though Figure 10 indicates that erosion and deposition rates were relatively constant throughout the flood, this is based on volume changes spatially integrated over the entire site areas and thus does not fully explain how changes occurred within the sites. For example, the styles of erosion can be seen more clearly on difference maps for specific time periods, particularly during the rising limb versus the flood peak (Figure 11). Both sites experienced substantial erosion along the channel-eddy interface during the rising limb that was likely the result of a combination of mass failures and bed shear stress divergence. It is well known that mass failures are common in sandbars in Grand Canyon and other similar environments [*Andrews et al.*, 1999; *Schmidt*, 1999; *Dexter and Cluer*, 1999; *Van Den Berg et al.*, 2002], and failures were observed directly in the field during surveying. However, these sudden failures are hidden in the cumulative changes (Figure 10) because the sand eroded from the bar slope was immediately deposited in the main channel and then gradually eroded during the flood peak (Figure 11, top right). At WT, less deposition occurred in the main channel as a result of sandbar slope erosion on the rising limb such that low-elevation erosion abated at the beginning of the flood peak (Figure 10, left).

[19] Deposition of sand on the reattachment and separation sandbars tended to occur gradually and consistently for most of the flood, as might be expected for shear stress divergence-based deposition from suspension. This is apparent in Figure 10 (right) and in the difference maps of Figure 11 where it is seen that deposition occurred on the sandbars during the rising limb and the flood peak. However, a mass failure was observed at the toe of the WT reattachment bar near the end of the flood and the remnants of this can be seen in Figure 11 (bottom right). The failure occurred very near the eddy eye, and the resulting deposition in the main channel is apparent (red area). Thus, it is likely that the processes of sudden erosion and gradual deposition are linked, whereby gradual deposition leads to oversteepening of the bar slopes and eventual mass failure.

4.3. Sand Capture Rates

[20] Because of the limited postdam sand supply to Grand Canyon [e.g., *Topping et al.*, 2000], the potential success of controlled floods for rebuilding sandbars depends on the rate at which the sandbars "capture" the sand that is available [*Wright et al.*, 2008]. That is, what percentage of the sand passing by the lateral recirculation zones is deposited on the sandbars versus being transported downstream? We evaluated this by computing the percentage of sand passing the sites that was captured, between each survey. The sand capture efficiency (percent) was defined as the volume of sand deposited at high elevation (above 227 m^3/s) at each site divided by the volume of sand transported through the main channel, during a given time interval. The volume of sand transported through the main channel was computed based on our suspended-sediment measurements by assuming that the measured concentrations (profiles at a single point in the middle of the channel) were representative of the cross

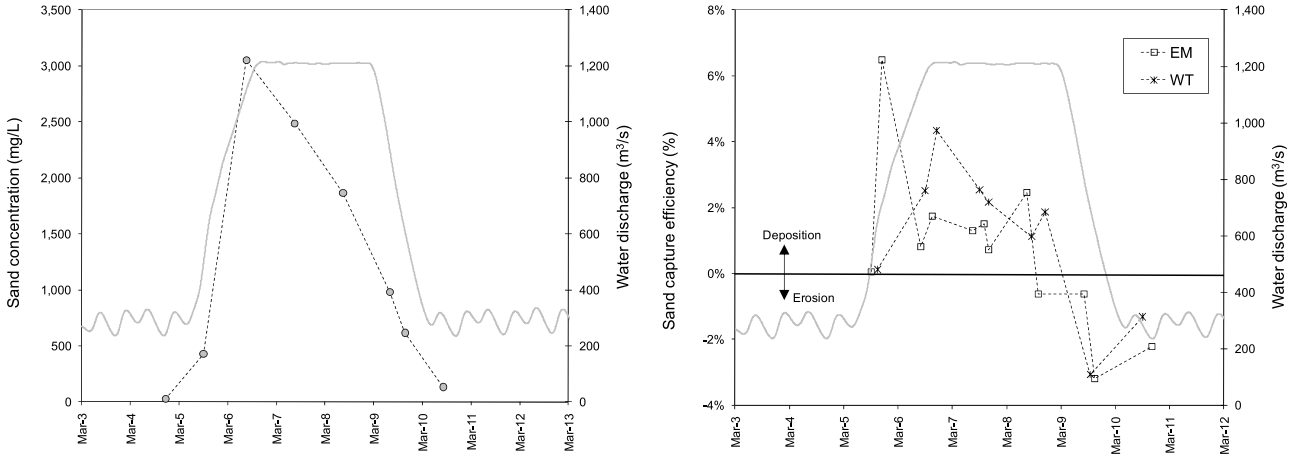

Figure 12. (left) Measured sand concentrations (circles) and (right) sand capture efficiency for both sites during the controlled flood.

section. The results are shown in Figure 12 (right), along with the sand concentration measurements (left). It is seen that concentrations peaked near the end of the rising limb and then decreased roughly linearly throughout the peak indicating sand supply limitation. At EM, the capture efficiency peaked (~6%) early on the rising limb and was then relatively constant (~2%) on the peak flow. Capture efficiency at WT was maximum (~4%) at the beginning of the peak flow and then gradually decreased down to about 2% at the end of the peak. These patterns support the link between sand concentration and sandbar deposition rates that has been noted by *Schmidt et al.* [1993], *Wiele et al.* [1999], and *Andrews and Vincent* [2007]. Because capture rates were negative (i.e., erosion) on the flood recession, summing over the flood duration yielded capture efficiencies of about 1% and 1.5% for EM and WT, respectively. These rates are much smaller than the *Schmidt et al.* [1993] flume studies where capture efficiencies decreased from 37% when the eddy was empty to 24% when the eddy was about 32% full. This suggests that our field sites were more closely in equilibrium with hydraulics and sand supply than the eddies in the flume experiments. We also note that the two sites represent a small percentage of the eddy sandbar area in the reach. For example, *Hazel et al.* [2006b] estimated the total area of eddies in Marble Canyon (Lees Ferry to Little Colorado River confluence, see Figure 1) to be about 2.6×10^6 m^2, which is about 50 times the area of our two study sites. We do not consider it appropriate to extrapolate our capture rates based on this area ratio; however, this information suggests that the rough estimate of 15% for Marble Canyon used by *Wright et al.* [2008] is reasonable but potentially somewhat low.

5. Discussion: Linking Flow Structures and Morphodynamics

[21] The observations of secondary flow structures and sandbar morphodynamics described above indicate several close linkages. First, as expected, the dominant link between flow structures and morphodynamics for our sites is the development of sandbars within the lateral recirculation zones. This link has been noted in other settings, such as sharply curved meander bends [*Hodskinson and Ferguson*, 1998] and groyne fields [*Sukhodolov et al.*, 2002], and has been studied extensively in Grand Canyon by *Schmidt* [1990], *Schmidt and Graf* [1990], *Rubin et al.* [1990], and *Schmidt et al.* [1993], among others. Fine sediment deposition occurs in these zones due to flow deceleration around the reattachment point and due to weak secondary circulation or stagnant flow immediately downstream from the separation point, leading to two distinct deposits termed reattachment and separation sandbars [*Schmidt*, 1990, Figure 2]. Sediment is exchanged between the recirculating eddies and the main channel by strong cross-stream velocities, in both directions.

[22] For our study sites, changes in flow rate during the controlled flood altered the flow structures and led to substantial morphologic changes. The general trend was for erosion to occur from the lower elevations within the recirculation zones where sand can accumulate during typical dam releases, accompanied by deposition at higher elevations near the reattachment and separation points. The main difference in response between the two sites was that substantially more erosion occurred at EM as compared to WT. We hypothesize that this was due to hydraulic differences between the two sites, as follows. At EM, the eddy lengthened substantially at high flow whereas at WT lengthening was limited due to the presence of a downstream debris fan. The lengthening at EM resulted in a zone of cross-stream flow reversal in the area where the majority of the erosion occurred (i.e., around the eddy eye). It is seen from Figure 6 that at transect EM4 the cross-stream flow switched from into the eddy at low flow to out of the eddy at high flow, due to the eye moving downstream. Thus we hypothesize that flow into the eddy is conducive to deposition during low flow, followed by erosion of the deposit when the cross-stream flow switches direction at high flow. This is supported by the subaqueous deposit apparent in the EM preflood bathymetry (Figure 8, top). Though the WT site also experienced erosion along the channel-eddy interface, it was substantially less and we speculate that this is due to the lack of cross-stream flow reversal at this site. However, because there are other differences between the sites that could potentially explain the disparity in low-elevation erosion (such as the approach angle of the flow into each site), our

hypothesis requires further testing. Numerical modeling may offer a promising avenue for systematically evaluating controls on erosion and deposition in these settings, similar to model applications to meander bends [*Hodskinson and Ferguson*, 1998], channel confluences [*Bradbrook et al.*, 1998] and pool-riffle units [*Booker et al.*, 2001].

[23] Though the links between lateral recirculation and sandbar morphology are clear and consistent with previous studies, the morphodynamic roles of the observed helical flow structures are more difficult to assess and have not been the subject of previous studies (due to a lack of 3D velocity measurements). In the return current channel (Figure 2), it seems likely that helical flow contributes to maintenance of the channel shape (e.g., Figure 7, transects WT7 and WT8). In this channel, near-bed cross-stream flow is oriented away from the "outer" bank and toward the reattachment sandbar thus contributing to scour of the channel and supplying sediment to the bar, similar to helical flow in a meander causing scour at the outer bed and supplying sediment to the point bar. However, flow must also accelerate away from the reattachment point into the return channel and this acceleration also likely contributes to scour and maintenance of the channel. The role of the helical flow in the main channel is even less clear. It seems unlikely that these structures are much of a factor in maintaining the scour hole in the main channel; these scour holes are more likely the result of the high-velocity flow emerging from the rapids. It is possible that these structures act similarly to the return channel structures by contributing to near-bed cross-stream velocities oriented toward the reattachment sandbar, thus enhancing sediment supply to the bars. Our observations provide some support for this hypothesis, but it is relatively thin. The best evidence for this is from transect EM6 (Figure 6) where cross-stream flow toward the sandbar in the center of the main channel is highest near the bed (where sediment concentrations are highest). It is also evident that in regions where the cross-stream flow is directed into the eddy, near-bed velocities tend to be slightly higher than near-surface velocities (Figures 6 and 7, transects EM5, EM6, EM7, WT6, WT7, WT8). Main channel helical flows may be a factor in this phenomenon; however, it seems more plausible that this is the result of topographically induced acceleration of cross-stream flow directed into the adverse sandbar slope. Unfortunately, the main channel helical flows were not sufficiently resolved by our measurements to draw definitive conclusions. Longer averaging times and potentially a finer spatial grid are likely necessary in this turbulent mixing zone to better resolve these structures.

6. Conclusions

[24] The secondary flow structures observed in two pool-rapid units along the Colorado River in Grand Canyon are similar to those that have been observed in many other types of river environments. At our study sites, large lateral recirculation zones developed downstream from the channel constrictions as a result of flow separation, and these structures were accompanied by helical flows both in the main channel and in the eddy return current channels (the main conduits of upstream flow). The helical flows resulted from the interaction between significant cross-stream velocities (arising from the lateral recirculation) and the channel boundaries, and thus share many attributes of helical flows in meander bends and downstream from channel confluences. Thus, our study adds to the long list of environments where lateral recirculation and helical flows have been observed, including straight channels, braided rivers, meander bends, channel confluences, pool-riffle units, and groyne fields and suggests that these structures are nearly ubiquitous in flows of water over complex topography at the river channel scale.

[25] Sandbar dynamics at our study sites were closely linked to the secondary flow structures. The lateral recirculation zones were conducive to fine sediment deposition, leading to building up of sandbar deposits around the reattachment point and in the area of flow separation. This deposition was accompanied by erosion along the sandbar slope at the interface with the main channel, where mass failures were observed. Helical flow structures were also likely linked to the sandbar dynamics, though in a secondary role to lateral recirculation. For example, helical flows in the return current channels likely contributed to channel scour and maintenance, and enhanced sand supply to the sandbars by directing near bed flow toward the reattachment bars. The helical flows in the main channel may play a similar role; however further study is required to better understand the morphodynamic consequences of these helical flows.

[26] The results of this study are relevant to the design of future controlled flood releases from Glen Canyon Dam. For example, our results confirm the basic process of using controlled floods to transfer sand from elevations below base flow, where it may accumulate during typical dam operations, to sandbars at elevations above base flow. Also, because of the limited postdam sediment supply, a key aspect of controlled floods is their efficiency in building sandbars. We have documented the capture efficiency at our two study sites and these results can be integrated with previous results to refine estimates of the potential for long-term maintenance of sandbars given the limited sand supply. Finally, predictive tools are needed to evaluate the expected efficiency of a given controlled flood hydrograph, and our measurements can be used to calibrate and test appropriate numerical models. Previously, hydraulic information was not available for evaluating models of the complex mixing processes that we have documented. Models can be used to evaluate a range of scenarios for controlled flood hydrographs, potentially improving the results of future floods. In addition to potentially benefiting resource management, numerical models may also prove useful for further study of the links between flow structures and morphodynamics in pool-rapid rivers.

[27] **Acknowledgments.** This study was funded by the U.S. Geological Survey's Grand Canyon Monitoring and Research Center and would not have been possible without a talented field crew consisting of Brian Dierker, Pete Weiss, Tim Cooper, Keith Kohl, Joe Hazel, Emily Thompson, Nathan Schott, Craig Anderson, and Kees Sloff. Ongoing discussions with the Grand Canyon "sediment team" contributed to design and outcomes of this study. Jack Schmidt and Joe Hazel provided helpful comments and discussions based on initial drafts of the manuscript. Two anonymous reviews and a review by Maarten Kleinhans led to substantial improvements to the manuscript.

References

Andrews, E. D., and K. R. Vincent (2007), Sand deposition in shoreline eddies along five wild and scenic rivers, Idaho, *River Res. Appl.*, *23*, 7–20, doi:10.1002/rra.960.

Andrews, E. D., C. E. Johnston, J. C. Schmidt, and M. Gonzales (1999), Topographic evolution of sandbars, in *The Controlled Flood in Grand Canyon*, *Geophys. Monogr. Ser.*, vol. 110, edited by R. H. Webb et al., pp. 117–130, AGU, Washington, D. C.

Ashmore, P. E., R. I. Ferguson, K. L. Prestegaard, P. J. Ashworth, and C. Paola (1992), Secondary flow in anabranch confluences of a braided, gravel-bed stream, *Earth Surf. Processes Landforms*, *17*, 299–311, doi:10.1002/esp.3290170308.

Bathurst, J. C., C. R. Thorne, and R. D. Hey (1977), Direct measurements of secondary currents in river bends, *Nature*, *269*, 504–506, doi:10.1038/269504a0.

Booker, D. J., D. A. Sear, and A. J. Payne (2001), Modelling three-dimensional flow structures and patterns of boundary shear stress in a natural pool-riffle sequence, *Earth Surf. Processes Landforms*, *26*, 553–576, doi:10.1002/esp.210.

Bradbrook, K. F., P. M. Biron, S. N. Lane, K. S. Richards, and A. G. Roy (1998), Investigation of controls on secondary circulation in a simple confluence geometry using a three-dimensional numerical model, *Hydrol. Processes*, *12*, 1371–1396, doi:10.1002/(SICI)1099-1085(19980630)12:8<1371::AID-HYP620>3.0.CO;2-C.

Bradbrook, K. F., S. N. Lane, and K. S. Richards (2000), Numerical simulation of three-dimensional, time-averaged flow structure at river channel confluences, *Water Resour. Res.*, *36*(9), 2731–2746, doi:10.1029/2000WR900011.

Calder, B. R., and L. A. Mayer (2003), Automated processing of high-rate, high-density multibeam echosounder data, *Geochem. Geophys. Geosyst.*, *4*(6), 1048, doi:10.1029/2002GC000486.

Dexter, L. R., and B. L. Cluer (1999), Cyclic erosional instability of sandbars along the Colorado River, Grand Canyon, Arizona, *Ann. Assoc. Am. Geogr.*, *89*, 238–266, doi:10.1111/1467-8306.00144.

Dietrich, W. E., and J. D. Smith (1983), Influence of the point bar on flow through curved channels, *Water Resour. Res.*, *19*(5), 1173–1192, doi:10.1029/WR019i005p01173.

Dietrich, W. E., and J. D. Smith (1984), Bed load transport in a river meander, *Water Resour. Res.*, *20*(10), 1355–1380, doi:10.1029/WR020i010p01355.

Dietrich, W. E., J. D. Smith, and T. Dunne (1979), Flow and sediment transport in a sand-bedded meander, *J. Geol.*, *87*, 305–315, doi:10.1086/628419.

Edwards, T. K., and D. G. Glysson (1999), *Field methods for measurement of fluvial sediment*, *Tech. Water Resour. Invest.*, Book 3, Chap. C2, 97 pp., U.S. Geol. Surv., Reston, Va. (Available at: http://pubs.usgs.gov/twri/twri3-c2/pdf/TWRI_3-C2.pdf)

Ferguson, R. I., D. R. Parsons, S. N. Lane, and R. J. Hardy (2003), Flow in meander bends with recirculation at the inner bank, *Water Resour. Res.*, *39*(11), 1322, doi:10.1029/2003WR001965.

Grams, P. E., and J. C. Schmidt (1999), Geomorphology of the Green River in the eastern Uinta Mountains, Dinosaur National Monument, Colorado and Utah, in *Varieties of Fluvial Form*, edited by A. J. Miller and A. Gupta, pp. 81–111, Wiley, Chichester, U. K.

Guy, H. P. (1969), *Laboratory Theory and Methods for Sediment Analysis*, *Tech. Water Resour. Invest.*, Book 5, Chap. C1, 59 pp., U.S. Geol. Surv., Reston, Va. (Available at: http://pubs.usgs.gov/twri/twri5c1/pdf/TWRI_5-C1.pdf)

Hazel, J. E., Jr., M. Kaplinski, R. Parnell, K. Kohl, and D. J. Topping (2006a), Stage-discharge relations for the Colorado River in Glen, Marble, and Grand Canyons, Arizona, 1990–2005, *U.S. Geol. Surv. Open File Rep., 2006-1243*, 7 pp.

Hazel, J. E., Jr., D. J. Topping, J. C. Schmidt, and M. Kaplinski (2006b), Influence of a dam on fine-sediment storage in a canyon river, *J. Geophys. Res.*, *111*, F01025, doi:10.1029/2004JF000193.

Hazel, J. E., Jr., M. Kaplinski, R. A. Parnell, K. Kohl, and J. C. Schmidt (2008), Monitoring fine-grained sediment in the Colorado River ecosystem, Arizona—Control Network and conventional survey techniques, *U.S. Geol. Surv. Open File Rep., 2008-1276*, 15 pp.

Hodskinson, A., and R. I. Ferguson (1998), Numerical modeling of separated flow in river bends: Model testing and experimental investigation of geometric controls on the extent of flow separation at the concave bank, *Hydrol. Processes*, *12*, 1323–1338, doi:10.1002/(SICI)1099-1085(19980630)12:8<1323::AID-HYP617>3.0.CO;2-S.

Howard, A. D., and R. Dolan (1981), Geomorphology of the Colorado River in the Grand Canyon, *J. Geol.*, *89*, 269–298, doi:10.1086/628592.

Kaplinski, M., J. E. Hazel Jr., R. Parnell, M. Breedlove, K. Kohl, and M. Gonzales (2009), Monitoring fine-sediment volume in the Colorado River ecosystem, Arizona: Bathymetric survey techniques, *U.S. Geol. Surv. Open File Rep., 2009-1207*, 33 pp.

Leeder, M. R., and P. H. Bridges (1975), Flow separation in meander bends, *Nature*, *253*, 338–339, doi:10.1038/253338a0.

Miller, A. J. (1994), Debris-fan constrictions and flood hydraulics in river canyons: Some implications from two-dimensional flow modeling, *Earth Surf. Processes Landforms*, *19*, 681–697, doi:10.1002/esp.3290190803.

Rhoads, B. L., and S. T. Kenworthy (1995), Flow structure at an asymmetrical stream confluence, *Geomorphology*, *11*, 273–293, doi:10.1016/0169-555X(94)00069-4.

Rubin, D. M., J. C. Schmidt, and J. N. Moore (1990), Origin, structure, and evolution of a reattachment bar, Colorado River, Grand Canyon, Arizona, *J. Sediment. Petrol.*, *60*(6), 982–991.

Schmidt, J. C. (1990), Recirculating flow and sedimentation in the Colorado River in Grand Canyon, Arizona, *J. Geol.*, *98*, 709–724, doi:10.1086/629435.

Schmidt, J. C. (1999), Summary and synthesis of geomorphic studies conducted during the 1996 controlled flood in Grand Canyon, in *The Controlled Flood in Grand Canyon*, *Geophys. Monogr. Ser.*, vol. 110, edited by R. H. Webb et al., pp. 329–341, AGU, Washington, D. C.

Schmidt, J. C., and J. B. Graf (1990), Aggradation and degradation of alluvial sand deposits, 1965 to 1986, Colorado River, Grand Canyon National Park, Arizona, *U.S. Geol. Surv. Prof. Pap.*, *1493*, 74 pp.

Schmidt, J. C., and D. M. Rubin (1995), Regulated streamflow, fine-grained deposits, and effective discharge in canyons with abundant debris fans, in *Natural and Anthropogenic Influences in Fluvial Geomorphology*, *Geophys. Monogr. Ser.*, vol. 89, edited by J. E. Costa et al., pp. 177–195, AGU, Washington, D. C.

Schmidt, J. C., D. M. Rubin, and H. Ikeda (1993), Flume simulation of recirculating flow and sedimentation, *Water Resour. Res.*, *29*(8), 2925–2939, doi:10.1029/93WR00770.

Schmidt, J. C., P. E. Grams, and R. H. Webb (1995), Comparison of the magnitude of erosion along two large regulated rivers, *Water Resour. Bull.*, *31*, 617–631.

Sukhodolov, A., W. S. J. Uijttewaal, and C. Engelhardt (2002), On the correspondence between morphological and hydrodynamical patterns of groyne fields, *Earth Surf. Processes Landforms*, *27*, 289–305, doi:10.1002/esp.319.

Szupiany, R. N., M. L. Amsler, J. L. Best, and D. R. Parsons (2007), Comparison of fixed-and moving-vessel flow measurements with an aDp in a large river, *J. Hydrol. Eng.*, *133*(12), 1299–1309, doi:10.1061/(ASCE)0733-9429(2007)133:12(1299).

Thompson, D. M., E. E. Wohl, and R. D. Jarrett (1996), A revised velocity-reversal and sediment-sorting model for a high-gradient, pool-riffle stream, *Phys. Geogr.*, *17*, 142–156.

Thorne, C. R., and S. Rais (1985), Direct measurements of secondary currents in a meandering sand-bed river, *Nature*, *315*, 746–747, doi:10.1038/315746a0.

Topping, D. J., D. M. Rubin, and L. E. Vierra Jr. (2000), Colorado River sediment transport: Pt. 1: Natural sediment supply limitation and the influence of Glen Canyon Dam, *Water Resour. Res.*, *36*(2), 515–542, doi:10.1029/1999WR900285.

Topping, D. J., J. C. Schmidt, and L. E. Vierra Jr. (2003), Computation and Analysis of the instantaneous-discharge record for the Colorado River at Lees Ferry, Arizona—May 8, 1921, through September 30, 2000, *U.S. Geol. Surv. Prof. Pap.*, *1677*, 118 pp.

Uijttewaal, W. S. J., D. Lehmann, and A. van Mazijk (2001), Exchange processes between a river and its groyne fields: Model experiments, *J. Hydrol. Eng.*, *127*(11), 928–936, doi:10.1061/(ASCE)0733-9429(2001)127:11(928).

Van Den Berg, J. H., A. Van Gelder, and D. R. Mastbergen (2002), The importance of breaching as a mechanism of subaqueous slope failure in fine sand, *Sedimentology*, *49*(1), 81–95, doi:10.1111/j.1525-139X.2006.00168.x-i1.

Vanoni, V. A. (Ed.) (1975), *Sedimentation Engineering*, *Man. Rep. Eng. Pract*, vol. 54, Am. Soc. of Civ. Eng., New York.

Vincent, K. R., and E. D. Andrews (2008), Depositional settings of sand beaches along whitewater rivers, *River Res. Appl.*, *24*, 771–788, doi:10.1002/rra.1079.

Webb, R. H., P. G. Griffiths, C. S. Magirl, and T. C. Hanks (2005), Debris flows in Grand Canyon and the rapids of the Colorado River, in *The State of the Colorado River Ecosystem in Grand Canyon*, edited by S. P. Gloss, J. E. Lovich, and T. S. Melis, *U.S. Geol. Surv. Circ.*, *1282*, 139–152.

Wheaton, J. M., J. Brasington, S. E. Darby, and D. A. Sear (2009), Accounting for uncertainty in DEMs from repeat topographic surveys: Improved sediment budgets, *Earth Surf. Processes Landforms*, *35*(2), 135–156.

Wiele, S. M., and E. R. Griffin (1997), Modifications to one-dimensional model of unsteady flow in the Colorado River through the Grand Canyon, Arizona, *U.S. Geol. Surv. Water Resour. Invest. Rep., 97-4046*, 17 pp.

Wiele, S. M., J. B. Graf, and J. D. Smith (1996), Sand deposition in the Colorado River in the Grand Canyon from flooding of the Little Colorado River, *Water Resour. Res.*, *32*(12), 3579–3596, doi:10.1029/96WR02842.

Wiele, S. M., E. D. Andrews, and E. R. Griffin (1999), The effect of sand concentration on depositional rate, magnitude, and location in the Colorado River below the Little Colorado River, in *The Controlled Flood in Grand Canyon*, *Geophys. Monogr. Ser.*, vol. 110, edited by R. H. Webb et al., pp. 131–145, AGU, Washington, D. C.

Wright, S. A., J. C. Schmidt, T. S. Melis, D. J. Topping, and D. M. Rubin (2008), Is there enough sand? Evaluating the fate of Grand Canyon sandbars, *GSA Today*, *18*(8), 4–10, doi:10.1130/GSATG12A.1.

M. Kaplinski, Department of Geology, Northern Arizona University, Box 4099, Flagstaff, AZ 86011, USA.

S. A. Wright, U.S. Geological Survey, 6000 J St., Placer Hall, Sacramento, CA 95819, USA. (sawright@usgs.gov)